

Cite this: *RSC Adv.*, 2015, 5, 49752

# A sensor for formaldehyde detection: luminescent metal–organic framework $[\text{Zn}_2(\text{H}_2\text{L})(2,2'\text{-bpy})_2(\text{H}_2\text{O})]_n$

Zhengyan Zhao, Juanyuan Hao, Xuedan Song, Suzhen Ren and Ce Hao\*

Density functional theory and time-dependent density functional theory methods have been used to investigate the hydrogen bonding between the Metal–organic framework  $[\text{Zn}_2(\text{H}_2\text{L})(2,2'\text{-bpy})_2(\text{H}_2\text{O})]_n$  and formaldehyde in the electronically excited state. The calculated geometric configuration,  $^1\text{H}$  NMR chemical shift and IR spectra of the hydrogen-bonded complex demonstrated that the hydrogen bond was strengthened in the excited state  $\text{S}_1$ . The strengthening of the hydrogen bond in the  $\text{S}_1$  state would lead to a luminescence decreasing phenomenon of  $[\text{Zn}_2(\text{H}_2\text{L})(2,2'\text{-bpy})_2(\text{H}_2\text{O})]_n$ , and the fluorescent rate constant of  $[\text{Zn}_2(\text{H}_2\text{L})(2,2'\text{-bpy})_2(\text{H}_2\text{O})]_n$  was decreased when encapsulating formaldehyde into it. Taken together, these results indicated that  $[\text{Zn}_2(\text{H}_2\text{L})(2,2'\text{-bpy})_2(\text{H}_2\text{O})]_n$  could be used for the detection of formaldehyde.

Received 23rd April 2015  
Accepted 29th May 2015

DOI: 10.1039/c5ra07373a

[www.rsc.org/advances](http://www.rsc.org/advances)

## Introduction

Metal–organic frameworks (MOFs) have emerged as an interesting class of crystalline materials, which are constructed from metal ions or clusters and organic ligands through self-assembly. MOFs have received considerable attention in recent years because of their many intriguing characteristics, including their high permanent porosity and large surface areas.<sup>1–3</sup> Since the first study concerning the luminescence properties of MOFs was published in 2002, there has been a significant year-on-year increase in the number of reports pertaining to luminescent MOFs.<sup>4</sup> According to the ISI Web of Science, luminescent MOFs account for approximately 10% of all the reported MOFs.<sup>5</sup> Luminescent MOFs have several advantages over other inorganic and organic luminescent materials in terms of their composition, structure and general properties.<sup>6</sup> Furthermore, it has been shown that luminescent MOFs exhibit molecular recognition and chemosensing properties towards a variety of different materials, including volatile organic molecules,<sup>7,8</sup> explosives,<sup>9,10</sup> metal ions<sup>11</sup> and anions.<sup>12</sup> Chen *et al.*<sup>13</sup> recently demonstrated that the zeolitic imidazolate framework (ZIF), ZIF-67 can be used as a gas sensor for the detection of formaldehyde. Furthermore, Yu *et al.*<sup>14</sup> synthesized a Cu(I)-MOF which they successfully used as an acute naked-eye colorimetric sensor for the detection of formaldehyde at levels as low as 0.016 ppm. Taken together, the results of these recent studies demonstrate that luminescent MOFs are promising materials for the detection of formaldehyde.

Formaldehyde is one of the most common and well known indoor pollutants, and it can cause numerous adverse health effects, including irritation of the eyes and respiratory system.<sup>15,16</sup> In 2004, the International Agency for Research on Cancer (IARC) defined formaldehyde as a group 1 human carcinogen that causes nasopharyngeal carcinoma.<sup>16,17</sup> Furthermore, exposure to formaldehyde has been associated with an increased risk of leukemia, especially myeloid leukemia.<sup>18,19</sup> Several techniques have been developed for the detection of formaldehyde, including spectroscopy, derivatization, high-performance liquid chromatography, voltammetry, amperometry, enzyme electrodes and solid-state sensors.<sup>16,20–24</sup> Luminescent MOFs, however, could be used as unique chemical sensors for the detection of formaldehyde because of their large specific surface area, good thermal stability, uniformly structured nanoscale cavities and the potential to further decorate their outer surface.<sup>6,25</sup>

MOF generally interact with formaldehyde through hydrogen bonding. Upon photoexcitation, hydrogen-bonded systems would cause different electronic states with significant differences in their charge distribution properties, and this process is known as hydrogen bonding dynamics.<sup>26,27</sup> Photoexcitation experiments of this type are generally monitored using femtosecond time-resolved vibrational spectroscopy techniques, but the information of photophysical properties and geometries is indirect and the spectral resolution for the femtosecond laser pulses is also limited.<sup>27,28</sup> There is therefore an urgent need for combining accurate quantum chemical calculations to resolve this issue in laser experiments.<sup>26</sup> Quantum chemical calculations based on density functional theory (DFT) and time-dependent density functional theory (TDDFT) have been identified as the effective methods for

State Key Laboratory of Fine Chemicals, Dalian University of Technology, Panjin campus 124221, China. E-mail: haoce@dlut.edu.cn; Fax: +86-411-84748086; Tel: +86-411-84986335

calculating the properties of hydrogen-bonded systems in the ground and excited states.<sup>29,30</sup>

Li *et al.*<sup>31</sup> used a hydrothermal method to synthesize the MOF  $[\text{Zn}_2(\text{H}_2\text{L})(2,2'\text{-bpy})_2(\text{H}_2\text{O})]_n$ , which was constructed from a symmetric triangular semirigid multicarboxylate ligand {3,3',3'-[1,3,5-phenylenetri(oxy)]triphthalic acid} and a 2,2'-bipyridine ligand using Zn(II) ions as the node. The authors also studied the luminescent properties of this MOF and reported that it produced a maximum luminescence peak at 371 nm upon photoexcitation at 300 nm. In our current study, DFT and TDDFT methods have been used to investigate the hydrogen bonding between  $[\text{Zn}_2(\text{H}_2\text{L})(2,2'\text{-bpy})_2(\text{H}_2\text{O})]_n$  and formaldehyde in the electronically excited state, as well as the luminescence mechanism of this material based on frontier molecular orbitals and electronic configuration. We also explored the effect of hydrogen bonding in the excited state on the rate constants of fluorescence and the possibility of using this MOF  $[\text{Zn}_2(\text{H}_2\text{L})(2,2'\text{-bpy})_2(\text{H}_2\text{O})]_n$  for the detection of formaldehyde.

### Computational details

Gaussian 09 suite of programs<sup>32</sup> were employed for geometry optimizations, IR spectra, UV-vis spectrum and <sup>1</sup>H NMR calculations by using the DFT and TDDFT methods. All of the above were calculated with the hybrid exchange–correlation functional using the Coulomb-attenuating method (CAM-B3LYP) functional.<sup>33</sup> For geometry optimizations and IR spectra calculations we used LANL2DZ basis sets,<sup>34</sup> while for <sup>1</sup>H NMR and UV-vis spectrum calculations we used 6-311++G(d,p) basis sets.<sup>35</sup> A scaling factor of 0.961 was utilized to calculate the IR spectra.<sup>36</sup>

ADF2012 program were employed to calculate the electronic configuration with the B3LYP hybrid functional and TZP basis sets.<sup>37,38</sup>

MOMAP package which was developed by Shuai's research group<sup>39–42</sup> were employed to calculate the rate constants of fluorescence.

## Results and discussions

### Geometric structure in the ground state

There is still no better solutions regarding to the calculation of periodic systems in the excited state. To simplify the computational processes, we selected a structure fragment by truncating from the periodic structure to represent the whole MOF. Fig. 1a shows the geometric configuration of the selected fragment (denoted as complex 1), which has a five-coordination connection with the Zn(II) ion in the center, as well as being surrounded by two benzoic acids, a hydrone and a 2,2'-bipyridine moiety. The encapsulation of formaldehyde into complex 1 at different sites would lead to the formation of different hydrogen-bonded complexes. We chose the lowest energy hydrogen-bonded complex for our further study, denoted as complex 2 (Fig. 1b). Complex 2 includes two hydrogen bonds (*i.e.*, C11=O10⋯H9–O5 and C13–O4⋯H12–C11), which are defined as HB-1 and HB-2, separately.

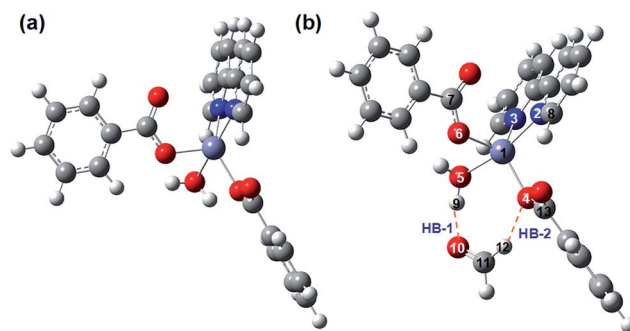


Fig. 1 (a) The geometric configuration of structure fragment denoted as complex 1. (b) Formaldehyde and complex 1 formed the most stable structure hydrogen-bonded complex denoted as complex 2, the orange dotted lines represent the hydrogen bonds HB-1 and HB-2 (purple: Zn atom; blue: N atom; red: O atom; gray: C atom; white: H atom).

The geometric optimization of complex 1 and its UV-vis spectrum were calculated using the DFT and TDDFT methods, respectively (Table 1). It is clear that the calculated values of the geometric structure and UV-vis spectrum are in good agreement with the experimental values.

The IR spectra of complex 1 and complex 2 were calculated in the ground state based on their corresponding optimized geometric structures, as shown in Fig. 2. The band at 752 cm<sup>−1</sup> in experimental is assigned to the bending vibration of the C–H bonds in benzene, with the corresponding band being observed at 749 cm<sup>−1</sup> of complex 1 and 753 cm<sup>−1</sup> of complex 2; the band at 1605 cm<sup>−1</sup> in experimental is assigned to the stretching vibration of the C=O bond of benzoic acid, with the corresponding band being observed at 1622 cm<sup>−1</sup> of complex 1 and 1623 cm<sup>−1</sup> of complex 2; the band at 3762 cm<sup>−1</sup> in experimental is assigned to the asymmetric stretching vibration of the O–H bond of hydrone, with the corresponding band being observed at 3755 cm<sup>−1</sup> of complex 1 and 3723 cm<sup>−1</sup> of complex 2. The

Table 1 The calculated and experimental values of geometric configuration and UV-vis spectrum of complex 1

	Cal. values	Exp. values <sup>31</sup>	Error
<b>Bond lengths/Å</b>			
Zn1–N2	2.13	2.09	0.04
Zn1–N3	2.11	2.12	−0.01
Zn1–O4	1.98	1.97	0.01
Zn1–O5	2.33	2.15	0.18
Zn1–O6	1.98	2.00	−0.02
O6–C7	1.33	1.32	0.01
<b>Bond angles/deg</b>			
N2–Zn1–N3	78.2	76.9	1.3
O6–Zn1–O5	77.4	77.3	0.1
N2–Zn1–O5	166.1	164.5	1.6
N3–Zn1–O6	110.0	109.9	0.1
Zn1–N2–C8	124.8	124.4	0.4
UV-vis maximum absorption/nm	285	300	15

results show that the calculated IR spectra of complex 1 and complex 2 are in good agreement with the corresponding experimental values. Besides, the band at  $3043\text{ cm}^{-1}$  of complex 2 is assigned to the stretching vibration of the C–H bond of formaldehyde, which demonstrate the existence of formaldehyde.

The calculated results for the geometry configuration, UV-vis spectrum and IR spectra are essentially consistent with the experiment values, which prove that the structure fragment we selected is reasonable and reliable.

### Frontier molecular orbitals and electronic configuration

A variety of different luminescence mechanisms have been reported for MOFs, including the metal-to-metal charge transfer, metal-to-ligand charge transfer, ligand-to-metal charge transfer, ligand-to-ligand charge transfer (LLCT), ligand-based luminescence and solvent-dependent luminescence mechanisms.<sup>4</sup> In our study, we focus on the fluorescence properties of luminescent MOF  $[\text{Zn}_2(\text{H}_2\text{L})(2,2'\text{-bpy})_2(\text{H}_2\text{O})]_n$ , so we mainly consider its singlet features. Based on Kasha's rule,<sup>43</sup> we only delineated the features of the lowest unoccupied molecular orbital (LUMO) and the highest occupied molecular orbital (HOMO) to reveal the nature of the charge transfer.

The frontier molecular orbitals of complex 1 and complex 2 are shown in Fig. 3. It is clear from Fig. 3a that the electron density distribution of the LUMO is mostly localized on the 2,2'-bipyridine group, whereas the electron density distribution of the HOMO is mostly localized on one of the benzoic acid groups. Fig. 3b shows that the electron density distribution of the LUMO in complex 2 is the same as that in complex 1, and HOMO is still localized on the same benzoic acid, but the positive and negative signs of the electron density are the complete opposite of those in complex 1. Encapsulating formaldehyde into complex 1 can affect its electronic density

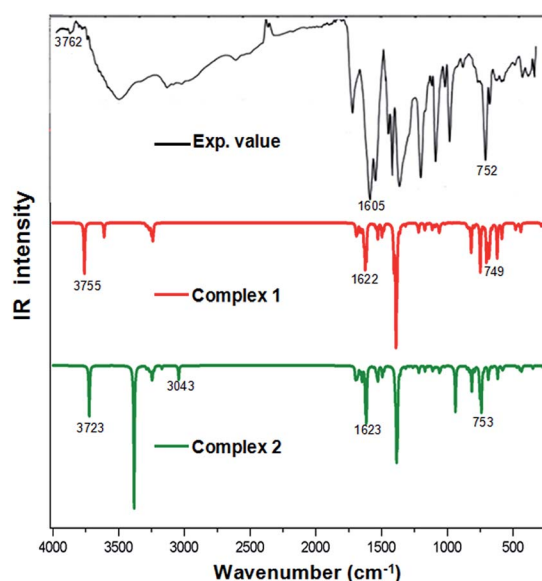


Fig. 2 The calculated IR spectra of complex 1 and complex 2 and experimental data<sup>31</sup> of  $[\text{Zn}_2(\text{H}_2\text{L})(2,2'\text{-bpy})_2(\text{H}_2\text{O})]_n$  in the ground state.

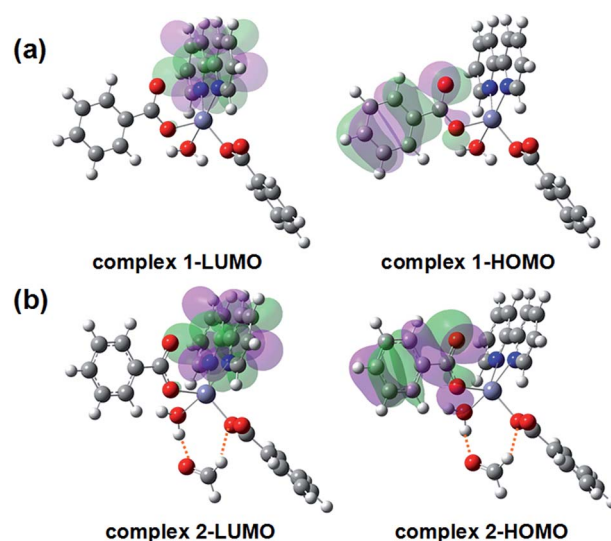


Fig. 3 The frontier molecular orbitals of (a) complex 1 and (b) complex 2 (green: positive sign; purple: negative sign).

distribution, which may affect the luminescence behavior of MOF  $[\text{Zn}_2(\text{H}_2\text{L})(2,2'\text{-bpy})_2(\text{H}_2\text{O})]_n$ .

Fig. 4 shows the frontier orbitals and electronic configuration of complex 2, as well as providing information pertaining to the contribution of each atomic orbital to the molecular orbital. The LUMO is mainly composed of the  $\pi^*$  orbital of C atom (74.9%) and N atom (25.5%) from the 2,2'-bipyridine ligand; the HOMO is mainly composed of the  $\pi$  orbital of C atom (5.8%) and n orbital of O atom (91.4%) from the benzoic acid ligand. However, the contributions of Zn atom to LUMO and HOMO are both 0%. Then we can conclude that the luminescence mechanism of complex 2 can be attributed to the ligand-to-ligand charge transfer (LLCT), with  $\pi^*-\pi$  and  $\pi^*-n$  characteristics. The result is therefore basically the same as the supposition of Li *et al.*<sup>31</sup>

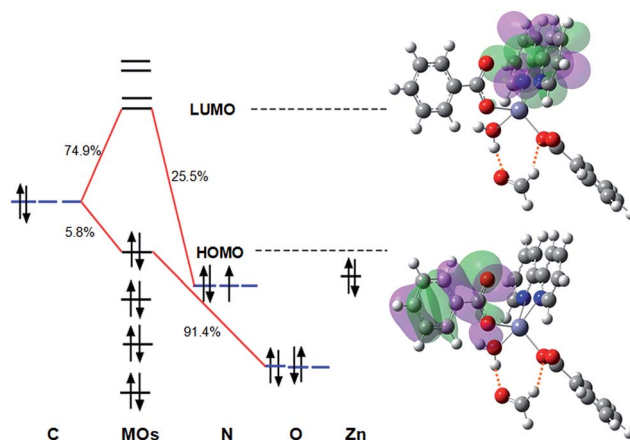


Fig. 4 The frontier molecular orbitals and electronic configuration of complex 2.

## Electronic excitation energies

Hydrogen bonding can have a significant impact on the way that a system behaves during electronic excitation, causes the hydrogen-bonded complex in different electronic states appear excellent difference in the charge distribution.<sup>44</sup> The electronic excitation energies of complexes 1 and 2 were calculated in several different electronic states using the TDDFT method, as the results were shown in Table 2. We mainly focus on the  $S_1$  state, and find that the electronic excitation energy of complex 2 in the  $S_1$  state is less than that of complex 1. In other words, the hydrogen bonding induces a red-shift in the electronic spectra, the rule is summarized by Zhao *et al.*<sup>26</sup> The guideline illustrates the relationship between the electronic spectral shifts and changes in hydrogen bonding in the excited states. If the hydrogen bonding in the electronic excited state is enhanced, it can induce a larger downshift of the excited-state energy level than that in the ground-state energy level, as a result, the energy gap between the excited state and ground state of the hydrogen-bonded system will decrease more than that of the system without hydrogen bond. Then we can conclude that the decrease in the electronic excitation energy from complex 1 to complex 2 in the  $S_1$  state effectively induces a red-shift in the electronic spectrum and also the hydrogen bond in the  $S_1$  state is strengthened.

## The behavior of hydrogen bonding in the electronically excited state

The behavior of hydrogen bonding in the electronically excited state is closely related to the luminescence behavior of MOF. By comparing the properties of hydrogen bond donor and acceptor systems in the  $S_0$  and  $S_1$  states, it is possible to develop a deeper understanding of the dynamic properties of hydrogen bonding in the  $S_1$  state.<sup>27</sup> In this study, the behavior of hydrogen bonding in complex 2 was evaluated based on three aspects, including the geometric configuration, the chemical shift of  $^1\text{H}$  NMR and IR spectra.

The geometric configuration of complex 2 in the  $S_1$  state was optimized using the TDDFT method. Table 3 shows the metric parameters of hydrogen bonds HB-1 and HB-2 of complex 2 in the  $S_0$  and  $S_1$  states. The length of HB-1 changes from 1.68 Å in

the  $S_0$  state to 1.80 Å in the  $S_1$  state, increased by 0.12 Å; whereas HB-2 changes from 2.14 Å in the  $S_0$  state to 1.74 Å in the  $S_1$  state, reduced by 0.4 Å. As for HB-1 ( $\text{C11}=\text{O10}\cdots\text{H9}-\text{O5}$ ), the bond length of  $\text{O10}\cdots\text{O5}$  is almost unchanged, and the bond angle of  $\text{O10}\cdots\text{H9}-\text{O5}$  is decreased, means that the bond length of  $\text{O10}\cdots\text{H9}$  is increased, which is consistent with the change of HB-1; for HB-2 ( $\text{C13}-\text{O4}\cdots\text{H12}-\text{C11}$ ), the bond length of  $\text{O4}\cdots\text{C11}$  is decreased, and the bond angle of  $\text{O4}\cdots\text{H12}-\text{C11}$  is increased, means that the bond length of  $\text{O4}\cdots\text{H12}$  is decreased, which is consistent with the change of HB-2. Since the observed length change in HB-1 is quite small and approach to the experimental error (0.1 Å), combined with the change of the electronic excitation energies that we conclude the hydrogen bond is enhanced in the  $S_1$  state, the length of HB-2 is dominant and is under our consideration in the current work.

The corresponding  $^1\text{H}$  NMR chemical shift of hydrogen atom H9 and H12 involved in HB-1 and HB-2 in the  $S_0$  and  $S_1$  states were calculated and listed in Table 3.<sup>45–48</sup> Since we only consider the length change in HB-2, then we focus on the  $^1\text{H}$  NMR chemical shift of H12. It can be clearly seen that the chemical shift of H12 decreased from 20.3 ppm in the  $S_0$  state to 17.1 ppm in the  $S_1$  state. The upfield shift means that the charge density around the nucleus of the hydrogen is increased, then the distance between the hydrogen atom and acceptor atom is decreased, means that the hydrogen bond HB-2 is enhanced,<sup>26</sup> which is in accordance with the bond length change of HB-2.

Monitoring the vibrational modes involved in the formation of hydrogen bond in the  $S_0$  and  $S_1$  states can provides an explicit understanding of the hydrogen bonding dynamics.<sup>26</sup> The IR spectra in the  $S_1$  state of complex 2 was calculated with the TDDFT method using the optimized geometric conformation of the excited state as the initial conformation. The stretching vibrational frequencies of the HB-2 donor C11–H12 and acceptor C13–O4 groups in the  $S_0$  and  $S_1$  states are shown in Fig. 5. The stretching frequency of the hydrogen bond donor C11–H12 shifted from  $3043\text{ cm}^{-1}$  in the  $S_0$  state to  $2694\text{ cm}^{-1}$  in the  $S_1$  state, representing a decrease of  $349\text{ cm}^{-1}$ ; the stretching

**Table 2** The electronic excitation energies of complex 1 and complex 2

Excited states	Complex 1 (eV)	Complex 2 (eV)
$S_1$	4.35	3.93
$S_2$	4.55	4.33
$S_3$	4.78	4.56
$S_4$	4.84	4.74
$S_5$	4.86	4.75
$S_6$	4.90	4.76
$S_7$	5.09	4.91
$S_8$	5.12	5.14
$S_9$	5.13	5.14
$S_{10}$	5.19	5.18

**Table 3** The calculated metric parameters of hydrogen bonds HB-1 and HB-2 and  $^1\text{H}$  NMR chemical shift of H9 and H12 of complex 2 in the  $S_0$  and  $S_1$  states

	$S_0$	$S_1$
<b>Bond lengths/Å</b>		
HB-1 ( $\text{C11}=\text{O10}\cdots\text{H9}-\text{O5}$ )	1.68	1.80
HB-2 ( $\text{C13}-\text{O4}\cdots\text{H12}-\text{C11}$ )	2.14	1.74
$\text{O10}\cdots\text{O5}$	2.67	2.68
$\text{O4}\cdots\text{C11}$	3.16	2.86
<b>Bond angles/deg</b>		
$\text{O10}\cdots\text{H9}-\text{O5}$	169.1	147.3
$\text{O4}\cdots\text{H12}-\text{C11}$	154.4	167.7
<b><math>^1\text{H}</math> NMR/ppm</b>		
H9	22.2	25.8
H12	20.3	17.1



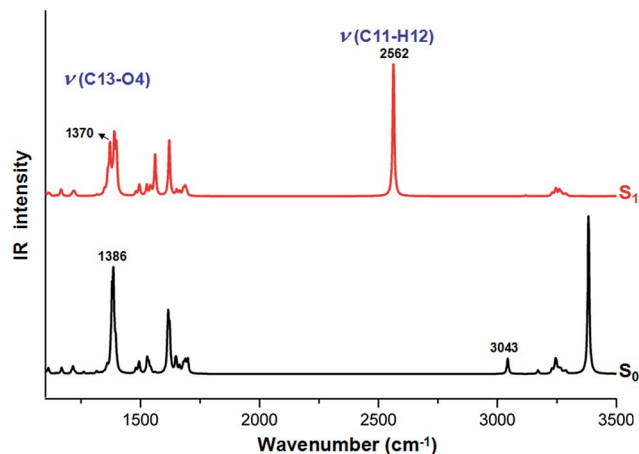


Fig. 5 Stretching vibration frequencies of C11–H12 and C13–O4 bonds.

frequency of the hydrogen bond acceptor C13–O4 shifted from 1386  $\text{cm}^{-1}$  in the  $S_0$  state to 1378  $\text{cm}^{-1}$  in the  $S_1$  state, representing a decrease of 8  $\text{cm}^{-1}$ . Both of these characteristic stretching frequencies are therefore red-shifted on going from the  $S_0$  state to the  $S_1$  state, which demonstrate that the hydrogen bond is increased in the  $S_1$  state.<sup>49</sup>

Thus, from the three aspects above, we have demonstrated that the hydrogen bond HB-2 was strengthened in the  $S_1$  state, which were consistent with the electronic excitation energies. The strengthening of HB-2 in the  $S_1$  state could therefore lead to a decrease in the quantum yield of the  $S_1$  state through deactivation and fluorescence, as reported by Zhao *et al.*<sup>26,50</sup> In this case, nonradiative decay process from the  $S_1$  state to the  $S_0$  state would become the main dissipative process of deactivation,<sup>51,52</sup> which would ultimately result in the rate of radiative decay process being decreased. Thus, the strengthened of the hydrogen bond HB-2 in the  $S_1$  state would therefore lead to a luminescence decreasing phenomenon of the MOF  $[\text{Zn}_2(\text{H}_2\text{L})(2,2'\text{-bpy})_2(\text{H}_2\text{O})]_n$ .

### The effect of hydrogen bonding in the electronically excited state on the fluorescent rate constants

With time-dependent perturbation theory and the Fermi-Golden rule, all kinds of the rate constant of deactivation process can be predicted through quantum chemistry calculation. The basic assumption is the Fermi-Golden rule modeled by displaced harmonic oscillator for two quantum states, which is derived based on the time-dependent perturbation theory. The expression of Fermi-Golden rule is:

$$k_{\text{if}} = \frac{2\pi}{\hbar} |\langle \varphi_i | V | \varphi_f \rangle|^2 \rho(E_f)$$

where  $i$  represents the initial state and  $f$  is the final state,  $V$  is electronic coupling depending on the nature of process, and  $\rho$  is the density of state (DOS).<sup>53</sup>

According to the Fermi-Golden rule, the radiative decay rate can be expressed as

Table 4 The calculated fluorescent rate constants of complex 1 and complex 2

	Complex 1	Complex 2
Fluorescent rate constants $k_{\text{r}}/\text{s}^{-1}$	$2.78 \times 10^6$	$1.12 \times 10^6$

$$k_{\text{r}(i0 \rightarrow f)} = \frac{64\pi^4}{3hc^3} |\mu|^2 \sum_a v_{i0 \rightarrow fa}^3 \left| \int \Theta_{fa}^* \Theta_{i0} dQ \right|^2$$

where  $v_{i0 \rightarrow fa}$  is the frequency of the spontaneous transition from the initial state (usually the first excited state) to the final state (usually the ground state);  $\mu$  is the electric transition dipole moment between the two states;  $\Theta_{i0}$  and  $\Theta_{fa}$  are the vibrational functions for the initial and final states, respectively;  $h$  is the Planck constant; and  $c$  is the speed of light in vacuum.<sup>39</sup>

We calculated the rate constants of the radiative decay process, mainly the fluorescent rate constants of complex 1 and complex 2 based on our former calculation, including geometry optimization, vibrational modes for the electronic ground and excited states. As shown in Table 4, the fluorescent rate constants are  $2.78 \times 10^6 \text{ s}^{-1}$  and  $1.12 \times 10^6 \text{ s}^{-1}$  for complex 1 and complex 2, respectively. Compared to complex 1, the fluorescent rate constant of complex 2 is decreased, namely, the fluorescence of MOF  $[\text{Zn}_2(\text{H}_2\text{L})(2,2'\text{-bpy})_2(\text{H}_2\text{O})]_n$  is weakened when encapsulating formaldehyde into it.

The recognition of a luminescent MOF for a guest molecule is mainly through the changes of its luminescence intensity.<sup>12</sup> Based on the luminescence weakened observed for  $[\text{Zn}_2(\text{H}_2\text{L})(2,2'\text{-bpy})_2(\text{H}_2\text{O})]_n$  with the encapsulation of formaldehyde, we consider that  $[\text{Zn}_2(\text{H}_2\text{L})(2,2'\text{-bpy})_2(\text{H}_2\text{O})]_n$  could be used as a chemical sensor for the detection of formaldehyde.

## Conclusions

By using DFT and TDDFT methods, we proved the structure fragment used in our study is reasonable in terms of the calculated results of the geometric structure, IR spectra and UV-vis spectrum. The calculated frontier molecular orbitals and electronic configuration revealed the mechanism of the luminescence was LLCT, with  $\pi^*-\pi$  and  $\pi^*-n$  characteristics. We also demonstrated the hydrogen bond was enhanced in the  $S_1$  state with the calculated results of geometric configuration,  $^1\text{H}$  NMR chemical shift and IR spectra, as well as the electronic excitation energies. The strengthening of the hydrogen bond in the  $S_1$  state would lead to a luminescence decreasing phenomenon of MOF  $[\text{Zn}_2(\text{H}_2\text{L})(2,2'\text{-bpy})_2(\text{H}_2\text{O})]_n$ . Besides, we also explored the effect of hydrogen bonding in the electronically excited state on the fluorescent rate constants and found the fluorescent rate constant of  $[\text{Zn}_2(\text{H}_2\text{L})(2,2'\text{-bpy})_2(\text{H}_2\text{O})]_n$  was decreased with the encapsulation of formaldehyde, which together indicated that the MOF  $[\text{Zn}_2(\text{H}_2\text{L})(2,2'\text{-bpy})_2(\text{H}_2\text{O})]_n$  could be used as a chemical sensor for formaldehyde detection.

The approach employed in our study could be used to identify other luminescent MOFs for the detection of formaldehyde and develop an in-depth understanding of the

mechanisms involved in the recognition and sensing of different molecules by luminescent MOFs.

## Acknowledgements

We acknowledge the financial support of the National Natural Science Foundation of China (Grants 21373042, 21036006 and 21137001) and the State Key Laboratory of fine chemicals (Panjin) project (Grant no. JH2014009), the Fundamental Research Funds for the Central Universities (Grant no. 1001852005).

## References

- H. C. Zhou, J. R. Long and O. M. Yaghi, *Chem. Rev.*, 2012, **112**, 673.
- H. C. Zhou and S. Kitagawa, *Chem. Soc. Rev.*, 2014, **43**, 5415.
- Z. J. Lin, J. Lü, M. Hong and R. Cao, *Chem. Soc. Rev.*, 2014, **43**, 5867.
- M. D. Allendorf, C. A. Bauer, R. K. Bhakta and R. J. T. Houk, *Chem. Soc. Rev.*, 2009, **38**, 1330.
- Y. Cui, Y. Yue, G. Qian and B. Chen, *Chem. Rev.*, 2011, **112**, 1126.
- Z. Hu, B. J. Deibert and J. Li, *Chem. Soc. Rev.*, 2014, **43**, 5815.
- L. E. Kreno, K. Leong, O. K. Farha, M. Allendorf, R. P. Van Duyne and J. T. Hupp, *Chem. Rev.*, 2011, **112**, 1105.
- M. J. Dong, M. Zhao, S. Ou, C. Zou and C. D. Wu, *Angew. Chem., Int. Ed.*, 2014, **53**, 1575.
- L. Liu, J. Y. Hao, Y. T. Shi, J. S. Qiu and C. Hao, *RSC Adv.*, 2015, **5**, 3045.
- A. K. Chaudhari, S. S. Nagarkar, B. Joarder and S. K. Ghosh, *Cryst. Growth Des.*, 2013, **13**, 3716.
- C. X. Yang, H. B. Ren and X. P. Yan, *Anal. Chem.*, 2013, **85**, 7441.
- B. Chen, L. Wang, F. Zapata, G. Qian and E. B. Lobkovsky, *J. Am. Chem. Soc.*, 2008, **130**, 6718.
- E. X. Chen, H. Yang and J. Zhang, *Inorg. Chem.*, 2014, **53**, 5411.
- Y. Yu, X. M. Zhang, J. P. Ma, Q. K. Liu, P. Wang and Y. B. Dong, *Chem. Commun.*, 2014, **50**, 1444.
- L. Feng, C. J. Musto and K. S. Suslick, *J. Am. Chem. Soc.*, 2010, **132**, 4046.
- T. Salthammer, S. Mentese and R. Marutzky, *Chem. Rev.*, 2010, **110**, 2536.
- V. Coglianò, Y. Grosse, R. Baan, K. Straif, M. Secretan and F. Glissassi, *Environ. Health Perspect.*, 2005, **113**, 1205.
- L. Zhang, L. E. B. Freeman, J. Nakamura, S. S. Hecht, J. J. Vandenberg, M. T. Smith and B. R. Sonawane, *Environ. Mol. Mutagen.*, 2010, **51**, 181.
- E. Schwillk, L. Zhang, M. T. Smith, A. H. Smith and C. Steinmaus, *J. Occup. Environ. Med.*, 2010, **52**, 878.
- Q. Meng, T. Han, G. Wang, N. Zheng, C. Cao and S. Xie, *Sens. Actuators, B*, 2014, **196**, 238.
- S. Srinives, T. Sarkar and A. Mulchandani, *Sens. Actuators, B*, 2014, **194**, 255.
- A. Nageswari, K. K. Reddy and K. Mukkanti, *Chromatographia*, 2012, **75**, 275.
- R. Knake, P. Jacquinot and P. C. Hauser, *Electroanalysis*, 2001, **13**, 631.
- Y. I. Korpan, O. O. Soldatkin, O. F. Sosovska, H. M. Klepach, E. Csöregi, F. Vocanson, N. Jaffrezic-Renault and M. V. Gonchar, *Microchim. Acta*, 2010, **170**, 337.
- Z. Y. Gu, C. X. Yang, N. Chang and X. P. Yan, *Acc. Chem. Res.*, 2012, **45**, 734.
- G. J. Zhao and K. L. Han, *Acc. Chem. Res.*, 2012, **45**, 404.
- G. J. Zhao and K. L. Han, *J. Phys. Chem. A*, 2007, **111**, 2469.
- G. Y. Li, G. J. Zhao, Y. H. Liu, K. L. Han and G. Z. He, *J. Comput. Chem.*, 2010, **31**, 1759.
- M. Ji, C. Hao, D. D. Wang, H. J. Li and J. S. Qiu, *Dalton Trans.*, 2013, 3464.
- A. L. Sobolewski and W. Domcke, *J. Phys. Chem. A*, 2004, **108**, 10917.
- N. Zhao, W. Li, C. Sun, Y. Bian, H. Wang, Z. Chang and H. Fan, *Solid State Sci.*, 2012, **14**, 317.
- M. J. Frisch, G. W. Trucks, H. B. Schlegel, G. E. Scuseria, M. A. Robb, J. R. Cheeseman, G. Scalmani, V. Barone, B. Mennucci, G. A. Petersson, H. Nakatsuji, M. Caricato, X. Li, H. P. Hratchian, A. F. Izmaylov, J. Bloino, G. Zheng, J. L. Sonnenberg, M. Hada, M. Ehara, K. Toyota, R. Fukuda, J. Hasegawa, M. Ishida, T. Nakajima, Y. Honda, O. Kitao, H. Nakai, T. Vreven, J. A. Montgomery Jr, J. E. Peralta, F. Ogliaro, M. Bearpark, J. J. Heyd, E. Brothers, K. N. Kudin, V. N. Staroverov, R. Kobayashi, J. Normand, K. Raghavachari, A. Rendell, J. C. Burant, S. S. Iyengar, J. Tomasi, M. Cossi, N. Rega, J. M. Millam, M. Klene, J. E. Knox, J. B. Cross, V. Bakken, C. Adamo, J. Jaramillo, R. Gomperts, R. E. Stratmann, O. Yazyev, A. J. Austin, R. Cammi, C. Pomelli, J. W. Ochterski, R. L. Martin, K. Morokuma, V. G. Zakrzewski, G. A. Voth, P. Salvador, J. J. Dannenberg, S. Dapprich, A. D. Daniels, Ö. Farkas, J. B. Foresman, J. V. Ortiz, J. Cioslowski and D. J. Fox, *Gaussian 09, revision A. 01*, Wallingford, CT, Gaussian, 2009.
- T. Yanai, D. P. Tew and N. C. Handy, *Chem. Phys. Lett.*, 2004, **393**, 51.
- P. J. Hay and W. R. Wadt, *J. Chem. Phys.*, 1985, **82**, 270.
- K. Raghavachari, J. S. Binkley, R. Seeger and J. A. Pople, *J. Chem. Phys.*, 1980, **72**, 650.
- NIST Computational Chemistry Comparison and Benchmark Database, NIST Standard Reference Database Number 101, Release 15b, August 2011, Editor Russell D. Johnson III, <http://cccbdb.nist.gov/>.
- G. Te Velde, F. M. Bickelhaupt, S. J. A. Van Gisbergen, C. Fonseca Guerra, E. J. Baerends, J. G. Snijders and T. Ziegler, *J. Comput. Chem.*, 2001, **22**, 931.
- C. F. Guerra, J. G. Snijders, G. Te Velde and E. J. Baerends, *Theor. Chem. Acc.*, 1998, **99**, 391.
- Q. Peng, Y. P. Yi, Z. G. Shuai and J. S. Shao, *J. Am. Chem. Soc.*, 2007, **129**, 9333.
- Q. Peng, Y. P. Yi, Z. G. Shuai and J. S. Shao, *J. Chem. Phys.*, 2007, **126**, 114302.
- Y. L. Niu, Q. Peng and Z. G. Shuai, *Sci. China, Ser. B: Chem.*, 2008, **51**, 1153.

- 42 Y. L. Niu, Q. Peng, C. M. Deng, X. Gao and Z. G. Shuai, *J. Phys. Chem. A*, 2010, **114**, 7817.
- 43 M. Kasha, *Discuss. Faraday Soc.*, 1950, **9**, 14.
- 44 G. J. Zhao, F. Yu, M. X. Zhang, B. H. Northrop, H. Yang, K. L. Han and P. J. Stang, *J. Phys. Chem. A*, 2011, **115**, 6390.
- 45 L. J. Altman and D. Laungani, *J. Am. Chem. Soc.*, 1978, **100**, 8264.
- 46 M. V. Vener, *Chem. Phys.*, 1992, **166**, 311.
- 47 S. N. Smirnov, N. S. Golubev, G. S. Denisov, H. Benedict, P. S. Mohammedi and H. H. Limbach, *J. Am. Chem. Soc.*, 1996, **118**, 4094.
- 48 P. M. Tolstoy, J. Guo, B. Koeppe, N. S. Golubev, G. S. Denisov, S. N. Smirnov and H. H. Limbach, *J. Phys. Chem. A*, 2010, **114**, 10775.
- 49 J. J. Tan, C. Hao, N. N. Wei, M. X. Zhang and X. Y. Dai, *J. Theor. Comput. Chem.*, 2011, **10**, 393.
- 50 G. J. Zhao and K. L. Han, *J. Phys. Chem. A*, 2007, **111**, 9218.
- 51 V. Samant, A. K. Singh, G. Ramakrishna, H. N. Ghosh, T. K. Ghanty and D. K. Palit, *J. Phys. Chem. A*, 2005, **109**, 8693.
- 52 L. Biczók, T. Bérces and H. Linschitz, *J. Am. Chem. Soc.*, 1997, **119**, 11071.
- 53 Z. G. Shuai and Q. Peng, *Phys. Rep.*, 2014, **537**, 123.